Observations of Mira stars with the IOTA/FLUOR interferometer and comparison with Mira star models

K.-H. Hofmann[a], U. Beckmann[a], T. Blöcker[a], V. Coude du Foresto[b], M. Lacasse[c], R. Millan-Gabet[c], S. Morel[c], B. Pras [c], C. Ruilier[b], D. Schertl[a], M. Scholz [d], V. Shenavrin[e], W. Traub[c], G. Weigelt[a], M. Wittkowski[a], B. Yudin[e]

[a]MPI für Radioastronomie, Auf dem Huegel 69, 53121 Bonn, Germany
[b]Observatoire de Paris-Meudon, 5 place Jules Janssen, 92195 Meudon Cedex, France
[c]Harvard-Smithsonian Center for Astrophysics, 60 Garden Street, Cambridge, Massachusetts 02138, USA
[d]Institut für Theoretische Astrophysik der Universitaet Heidelberg,Tiergartenstrasse 15, 69121 Heidelberg, Germany
[e] Sternberg Astronomical Institute, Universitetskii pr. 13, 119899 Moscow, Russia.

ABSTRACT

We present K-band observations of five Mira stars with the IOTA interferometer. The interferograms were obtained with the FLUOR fiber optics beam combiner which provides high-accuracy visibility measurements in spite of time-variable atmospheric conditions. For the Mira stars X Oph, R Aql, RU Her, R Ser, and V CrB we derived the uniform-disk diameters 11.7 mas, 10.9 mas, 8.4 mas, 8.1 mas, and 7.9 mas ($\pm$0.3 mas), respectively. Simultaneous photometric observations yielded the bolometric fluxes. The derived angular Rosseland radii and the bolometric fluxes allowed the determination of effective temperatures. For instance, the effective temperature of R Aql was determined to be 3072 K $\pm$161 K. A Rosseland radius for R Aql of 250 $R_\odot$ $\pm$63 $R_\odot$ was derived from the angular Rosseland radius of 5.5 mas $\pm$0.2 mas and the HIPPARCOS parallax of 4.73 mas $\pm$1.19 mas. The observations were compared with theoretical Mira star models[1,2] (D/P model Rosseland radius = 255 $R_\odot$; measured R Aql Rosseland radius = 250 $R_\odot$ $\pm$63 $R_\odot$).

Keywords: interferometry, Mira variables

1. INTRODUCTION

The resolution of large optical telescopes and interferometers is high enough to resolve the stellar disk of nearby M giant stars, to reveal photospheric asymmetries and surface structures, and to study the dependence of the diameter on the wavelength, variability phase, and cycle. Previous speckle or long-baseline interferometry observations were, for example, reported in Refs. 3-10. Theoretical studies (e.g. Refs. 1-2 and 11-13) show that accurate monochromatic diameter measurements can significantly improve our understanding of M giant atmospheres. With the IOTA interferometer a resolution of $\sim$9 mas can be achieved with its largest baseline of 38 m in the K-band. The IOTA interferometer is located at the Smithsonian Institution's Whipple Observatory on Mount Hopkins in Arizona. A detailed description of IOTA can be found in Refs. 14 and 15. IOTA can be operated in the K-band with the FLUOR[16] fiber optics beam combiner. This beam combiner provides high-accuracy visibility measurements in spite of time-variable atmospheric conditions. The single-mode fibers in the beam combiner spatially filter the wavefronts corrugated by atmospheric turbulence (see Refs. 16 and 17).

2. OBSERVATIONS

The five Miras X Oph, R Aql, RU Her, R Ser, V CrB were observed with the IOTA interferometer on May 16, 17 and 18, 1999. The observations were carried out with the fiber optics beam combiner FLUOR in the K-band and with 38 m baseline. The interferograms are scanned by the delay line during the coherence time of the atmosphere. The OPD length of the scan is $\sim 100\,\mu$m. Approximately 100 scans per baseline were recorded. Several reference stars (Table 1) were observed for the calibration of the observations (see Ref. 17 for more details). The diameters of the reference stars were derived from the scale of stellar diameters at K-magnitude = 0 for giants by Dyck et al.[18]. The fringe visibility of the reference stars was 64% - 94%. Fig. 1 shows the obtained visibility functions of the five Mira stars together with uniform-disk fits. The errors of the derived Mira star diameters are 1-3%.

Table 1. Observed data.

Star	spectral type	P [days]	Date	$\Phi_{\rm vis}$	$B_{\rm p}$ [m]	V	$\Theta_{\rm UD}$ [mas]	reference stars
X Oph	M5e-M9e	328	99 May 17	0.71	35.47	0.2317±0.024	11.74±0.30	HIP 86742
			99 May 18		34.75	0.2554±0.027		HIP 98337
			99 May 18		34.57	0.2279±0.025		HIP 98438
								HIP 97278
								HIP 97278
R Aql	M5e-M9e	284	99 May 17	0.17	35.42	0.2927±0.027	10.90±0.33	HIP 86742
			99 May 18		34.48	0.3295±0.031		HIP 98337
								HIP 98438
								HIP 97278
RU Her	M6e-M9	484	99 May 17	0.07	37.95	0.4768±0.017	8.36±0.20	HIP 71053
					37.73	0.4769±0.017		HIP 78159
R Ser	M5e-M9e	356	99 May 18	0.28	35.74	0.5467±0.016	8.10±0.20	HIP 61658
								HIP 75530
								HIP 85934
V CrB	C6,2e(N2e)	357	99 May 16	0.07	37.78	0.5288±0.017	7.86±0.24	HIP 73555
					38.02	0.5180±0.023		HIP 81833

In Table 1 the calibrated visibilities and the derived uniform-disk diameters of the five Miras are listed, together with observational parameters (spectral type, variability period P, date of observation, variability phase Φ_{vis}, projected baseline length $B_{\rm p}$, calibrated visibilities V, derived uniform-disk diameters $\Theta_{\rm UD}$, and reference stars).

3. COMPARISON OF THE OBSERVATIONS WITH MIRA STAR MODELS

In this section we derive angular diameters from the measured visibilities by fitting different theoretical center-to-limb intensity variations (hereafter CLV) of different Mira star models (Bessel, Scholz and Wood 1996 = BSW96[1], Hofmann, Scholz and Wood 1998 = HSW98[2]). From these angular diameters and the bolometric flux, we derive effective temperatures. For R Aql a HIPPARCOS parallax is available which allows us to determine linear radii. The comparison of these measured stellar parameters with theoretical ones indicate whether any of the models are a fair representation of the observed Mira stars. All Mira star models used in this paper are from BSW96 (D and E series) and from HSW98 (P, M and O series). They were developed as possible representations of the prototype Mira variable o Ceti, and hence have periods P very close to the 332 day period of this star; they differ in pulsation mode, assumed mass M and assumed luminosity L; and the BSW96 models differ from the (more advanced) HSW98 models with respect to the pulsation modelling technique. The five models represent stars pulsating in the fundamental mode (f; D, P and M models) or in the first-overtone mode (o; E and O models). Table 2 lists the properties of these Mira model series ($R_{\rm p}$ = Rosseland radius of the non-pulsating parent star of the Mira variable = distance from the "parent star's" center, at which the Rosseland optical depth $\tau_{\rm Ross}$ equals unity, see BSW96 and HSW98; $T_{\rm eff} \propto (L/R_{\rm p}^2)^{1/4}$ = effective temperature). Table 3 provides the link between the 22 abscissa values (model-phase combinations m) in Figs. 2 and 3, and the models, and it additionally lists the variability phase, relative Rosseland and stellar K-band filter radius, and the effective temperature. We compare predictions of these models at different phases and cycles with our observations.

Monochromatic radius R_λ and Rosseland radius R. We use the conventional stellar radius definition where the monochromatic radius R_λ of a star at wavelength λ is given by the distance from the star's center at which the optical depth equals unity ($\tau_\lambda = 1$). In analogy, the photospheric stellar radius R (Rosseland radius) is given by the

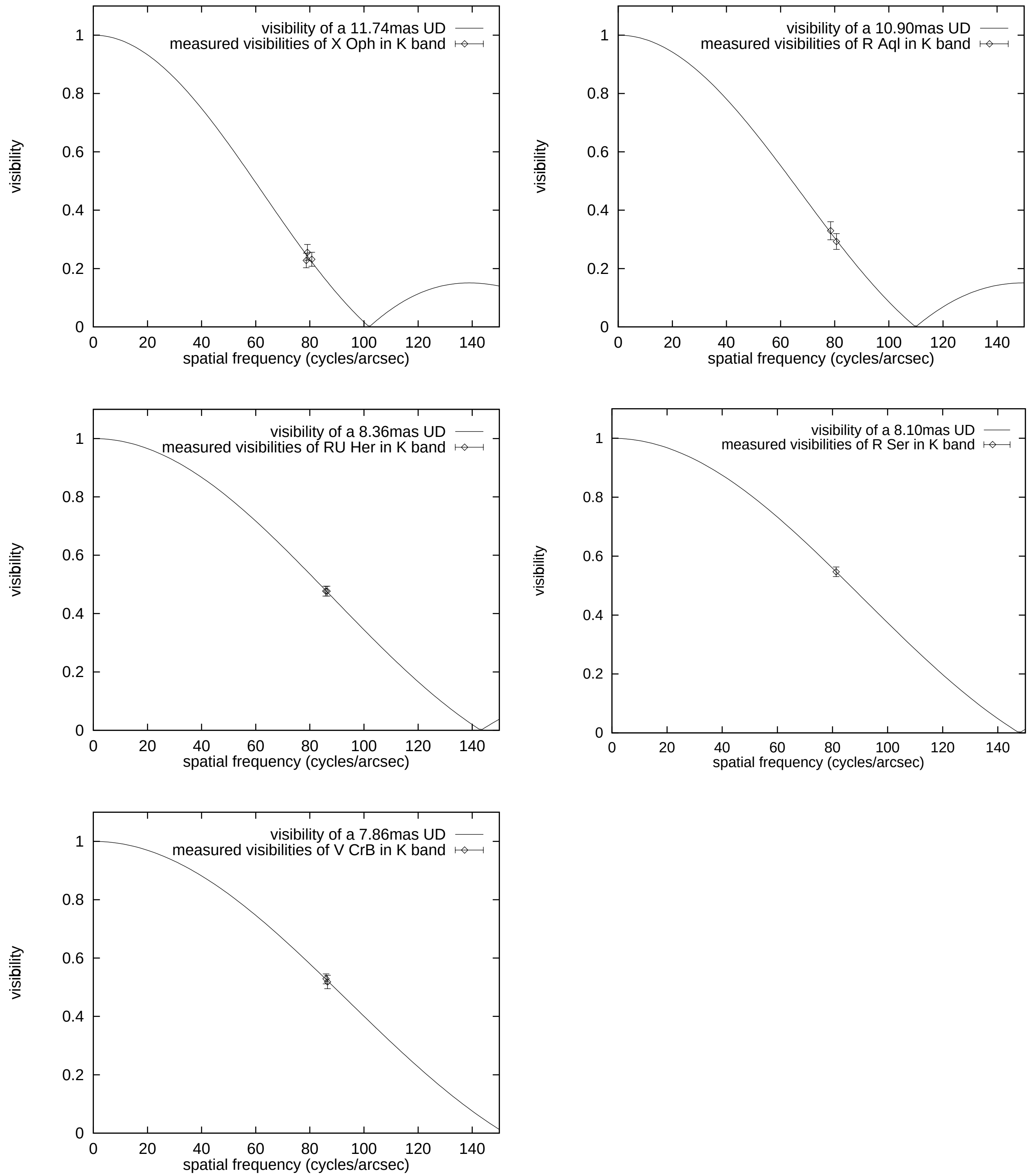

Figure 1. Uniform-disk fits (X Oph, R Aql, RU Her, R Ser, and V CrB).

Table 2. Properties of Mira model series[1,2] (see text)

Series	Mode	P(days)	$M/M_\odot$	$L/L_\odot$	$R_p/R_\odot$	T_{eff}/K
D	f	330	1.0	3470	236	2900
E	o	328	1.0	6310	366	2700
P	f	332	1.0	3470	241	2860
M	f	332	1.2	3470	260	2750
O	o	320	2.0	5830	503	2250

Table 3. Link between the 22 abscissa values (model-phase combinations m) in Figs. 2 and 3, and the models. The variability phase Φ_{vis}, the Rosseland radius R and the K-band radius R_K in units of the parent star radius R_p, and the effective temperature $T_{\text{eff}}(R)$ associated to the Rosseland radius are additionally given.

Model	Φ_{vis}	R/R_p	R_K/R_p	$T_{\text{eff}}(R)$	m
D27520	1+0.0	1.04	1.02	3020	1
D27760	1+0.5	0.91	0.90	2710	2
D28760	2+0.0	1.04	1.02	3030	3
D28960	2+0.5	0.91	0.91	2690	4
E8300	0+0.83	1.16	1.14	2330	5
E8380	1+0.0	1.09	1.10	2620	6
E8560	1+0.21	1.17	1.14	2610	7
P71800	0+0.5	1.20	1.04	2160	8
P73200	1+0.0	1.03	0.99	3130	9
P73600	1+0.5	1.49	1.12	1930	10
P74200	2+0.0	1.04	1.11	3060	11
P74600	2+0.5	1.17	1.02	2200	12
P75800	3+0.0	1.13	1.06	3060	13
P76200	3+0.5	1.13	0.96	2270	14
P77000	4+0.0	1.17	1.14	2870	15
M96400	0+0.5	0.93	0.92	2310	16
M97600	1+0.0	1.19	1.15	2750	17
M97800	1+0.5	0.88	0.90	2460	18
M98800	2+0.0	1.23	1.19	2650	19
O64210	0+0.5	1.12	1.09	2050	20
O64530	0+0.8	0.93	0.95	2150	21
O64700	1+0.0	1.05	1.01	2310	22

distance from the star's center at which the Rosseland optical depth equals unity ($\tau_{\text{Ross}} = 1$). This radius has the advantage of agreeing well (see Table 6 and the discussion in HSW98 for deviations sometimes occurring in very cool stars) with measurable near-infrared continuum radii and with the standard boundary radius of pulsation models with $T_{\text{eff}} \propto (L/R^2)^{1/4}$.

Stellar filter radius R_f. For the K-band filter used for the observations we have calculated the theoretical CLVs corresponding to the above mentioned five Mira star models at different phases and cycles. The stellar radius for filter transmission f_λ is the intensity and filter weighted radius $R_f = \int R_\lambda I_\lambda f_\lambda \, d\lambda \,/ \int I_\lambda f_\lambda \, d\lambda$, which we call stellar filter radius R_f after the definition of Scholz & Takeda[19]. In this equation R_λ denotes the above monochromatic $\tau_\lambda = 1$ radius, I_λ the central intensity spectrum and f_λ the transmission of the filter.

Observed angular stellar K-band radius $R^a_{\rm K,m}$ and observed angular Rosseland radius $R^a_{\rm m}$. The observed angular stellar K-band radii $R^a_{\rm K,m}$ of the observed Miras corresponding to the model-phase combinations m (see Table 3), were derived by least-squares fits between the measured visibilities and the visibilities of the corresponding theoretical CLVs. Additionally, the angular Rosseland radii $R^a_{\rm m}$ were derived from the obtained stellar K-band radii $R^a_{\rm K,m}$ and the theoretical ratios $R_{\rm m}/R_{\rm K,m}$ from Table 3 (Table 3 provides theoretical R and $R_{\rm K}$ values for each model-phase combination m). In the following subsections we apply CLVs predicted from all five models at phases both near our observations and, for comparison, also at other phases.

3.1. Effective temperature

Effective temperatures of each observed Mira star were derived from its angular Rosseland radii $R^a_{\rm m}$ and its bolometric flux using the relation

$$T_{\rm eff} = 2341\ {\rm K} \times (F_{\rm bol}/\phi^2)^{1/4} \tag{1}$$

where $F_{\rm bol}$ is the apparent bolometric flux in units of $10^{-8}\,{\rm erg\,cm^{-2}\,s^{-1}}$ and $\phi = 2\times R^a_{\rm m}$ is the angular Rosseland diameter in mas. The bolometric flux was derived from JHKLM-band observations carried out twelve days after the visibility observations. For cool stars such as LPVs, where most of the luminosity is emitted at near-infrared wavelengths, a convenient approximation for calculating bolometric magnitudes is to use a blackbody function to interpolate between photometric observations in the J, H, K, L and M bands. For estimating the bolometric flux we used JHKLM photometric measurements which were carried out with the 1.25 m telescope at the Crimean station of the Sternberg Astronomical Institute in Moscow twelve days after our visibility observations.

Fig. 2 shows a comparison of the measured and theoretical effective temperatures. Table 4 lists the measured bolometric flux and the average measured effective temperature for each of the five observed Mira stars. For R Aql we also derived effective temperatures for the best-fitting D and P models:

Measured effective temperature of R Aql:	3007±155 K	(D model*);	3109±168 K	(P model**)
Theoretical D and P model effective temperature:	3025 K	(D model*);	3030 K	(P model**)

(* average over phases 1.0, 2.0; ** average over phases 1.0, 2.0, 3.0, 4.0)

Table 4. Observational data and measured effective temperatures.

Star	Date	$\Phi_{\rm vis}$	K [mag]	$F_{\rm bol}$ [10^{-8} erg/cm^2 s]	$T_{\rm eff}$ [K]
X Oph	99 May 27	0.71	-0.83	320.6±50.1	2926±152**
R Aql	99 May 28	0.17	-0.86	351.2±52.7	3072±161*
RU Her	99 May 21	0.07	-0.11	159.8±24.0	2959±152*
R Ser	99 May 21	0.28	0.02	170.2±25.5	3112±160**
V CrB	99 May 27	0.07	0.96	52.8±8.0	2325±122*

(* average over all near-maximum model-phase combinations m since the phase of the observation was near-maximum)
(** average over all model-phase combinations m since models with phases close to the observation do not exist)

3.2. Linear radii

We have derived linear stellar K-band radii $R_{\rm K,m}$ and Rosseland radii $R_{\rm m}$ of R Aql from the measured angular stellar K-band radii $R^a_{\rm K,m}$ and Rosseland radii $R^a_{\rm m}$ by using the R Aql HIPPARCOS parallax of 4.73±1.19 mas[20]. The HIPPARCOS parallaxes of the other four observed Miras have too large errors for estimating useful linear radii. Fig. 3 shows the obtained linear Rosseland radii $R_{\rm m}$ and stellar K-band radii $R_{\rm K,m}$ of R Aql for all model-phase combinations m. The theoretical Rosseland radii of the D, M and P model series at all available near-maximum phases are close (within the error bars) to the measured Rosseland radii of R Aql. The theoretical Rosseland radii of the first-overtone models E and O are clearly too large compared with measured Rosseland radii. The same conclusions are also valid for the linear stellar filter radii $R_{\rm K}$ (Fig. 3).

If we calculate average R Aql radii by averaging the radii derived with all available *near-maximum* D model CLVs (i.e., m = 1, 3) and/or *near-maximum* P model CLVs (i.e., m = 9, 11, 13, 15) we obtain:

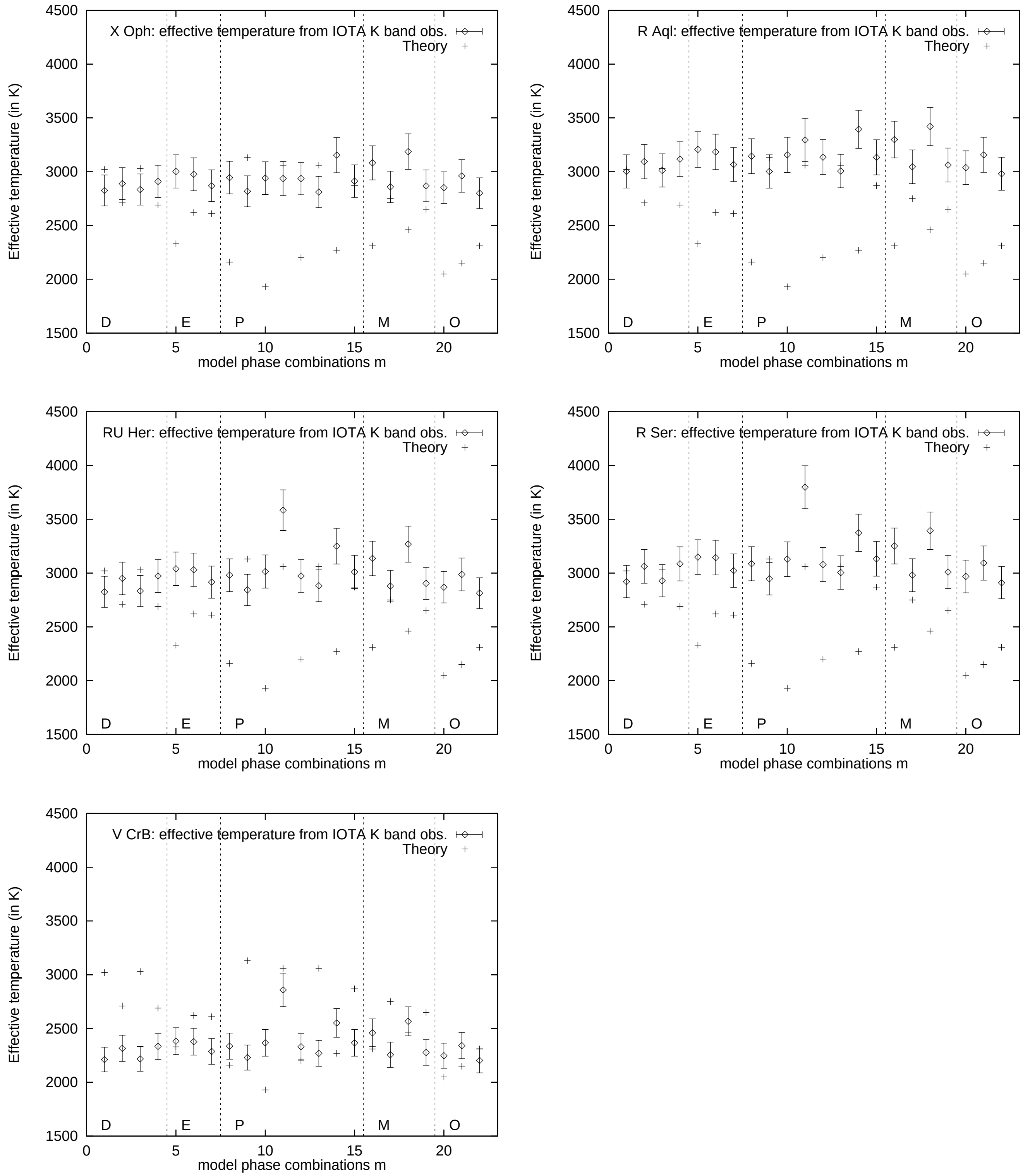

Figure 2. Comparison of measured effective temperatures of the 5 observed Mira stars and the theoretical model effective temperatures (see text). Table 3 shows the link between the abscissa values and the models and their phases.

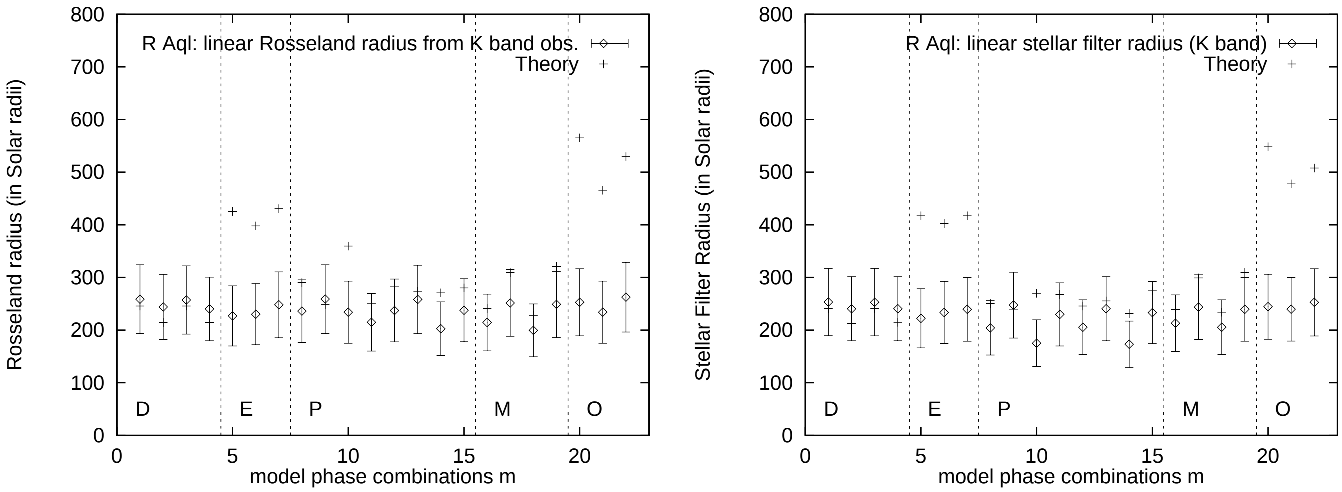

Figure 3. Comparison of measured R Aql radii and theoretical model radii: (left) linear Rosseland radii R_{m} and (right) linear stellar K-band radii $R_{\mathrm{K,m}}$ for all 22 model-phase combinations m. Table 3 gives the link between the abscissa values (model-phase combinations m) and the models and their phases.

Average theoretical D model Rosseland radius:	$246\,\mathrm{R}_\odot$	
Average measured D model R Aql Rosseland radius:	$258\,\mathrm{R}_\odot \pm 65\,\mathrm{R}_\odot$	(obtained with m = 1 and 3)
Average theoretical P model Rosseland radius:	$263\,\mathrm{R}_\odot$	
Average measured P model R Aql Rosseland radius:	$242\,\mathrm{R}_\odot \pm 61\,\mathrm{R}_\odot$	(obtained with m = 9, 11, 13 and 15)
Average theoretical D/P model Rosseland radius:	$255\,\mathrm{R}_\odot$	
Average measured D/P model R Aql Rosseland radius:	$250\,\mathrm{R}_\odot \pm 63\,\mathrm{R}_\odot$	(obtained with m = 1, 3, 9, 11, 13, 15, 17, 19; D and P models)

3.3. Pulsation mode

Adopting the above phase-averaged (over models D and P at maximum phases) linear Rosseland radius of $250\,\mathrm{R}_\odot \pm 63\,\mathrm{R}_\odot$ for R Aql, we find for the pulsation constant $Q = P\,(M/M_\odot)^{1/2}\,(R/R_\odot)^{-3/2}$ a value of Q=0.072±0.027 for a $1\,\mathrm{M}_\odot$-Mira with period P=284 days. This Q value agrees within the 1σ error with the theoretical value (Q=0.088) for fundamental pulsation mode for $1\,\mathrm{M}_\odot$-AGB stars with a period of ~ 284 days[21]. The corresponding Q value of first overtone pulsation mode is Q=0.049. Note, however, that no direct measurement of a Mira mass exists and that a 20% uncertainty of M would for example result in a 10% uncertainty of Q.

4. DISCUSSION

We derived the following angular uniform-disk diameters ϕ of five Mira stars from K-band visibility measurements with the 38 m baseline of the IOTA interferometer and the FLUOR beam combiner:

X Oph:	$\phi = 11.7$ mas ± 0.3 mas
R Aql:	$\phi = 10.9$ mas ± 0.3 mas
RU Her:	$\phi = 8.4$ mas ± 0.2 mas
R Ser:	$\phi = 8.1$ mas ± 0.2 mas
V CrB:	$\phi = 7.9$ mas ± 0.2 mas

The following effective temperatures were obtained from photometric JHKLM observations and the derived angular Rosseland radii:

X Oph	($\Phi_{\rm vis}$=0.71):	2926 K ±152 K
R Aql	($\Phi_{\rm vis}$=0.17):	3072 K ±161 K
RU Her	($\Phi_{\rm vis}$=0.07):	2959 K ±152 K
R Ser	($\Phi_{\rm vis}$=0.28):	3112 K ±160 K
V CrB	($\Phi_{\rm vis}$=0.07):	2325 K ±122 K

Previous interferometric K-band observations of some of our target stars (R Aql, X Oph, R Ser) were carried out by van Belle et al.[8] at similar phases. Their derived uniform-disk diameters (R Aql; $\Phi_{\rm vis} = 0.90$: 10.76±0.61 mas, X Oph; $\Phi_{\rm vis} = 0.75$: 12.30±0.66 mas, R Ser; $\Phi_{\rm vis} = 0.32$: 8.56±0.58 mas) are in good agreement with our observations (within the error bars). Their measured effective temperatures (R Aql: 3189±147 K, X Oph: 3041±160 K, R Ser: 2804±144 K) are also in good agreement with our results, with the exception of R Ser.

For R Aql a good HIPPARCOS parallax (4.73±1.19 mas) is available and it is therefore possible to compare measured linear Rosseland and stellar K-band radii with the theoretical radii of the BSW96 and HSW98 models. The measured radii were derived by fitting theoretical (BSW96, HSW98) center-to-limb intensity variations to the visibility data. In the following table we compare measured and theoretical values:

Measured linear R Aql Rosseland radii $R_{\rm m}$:	258±65 $R_\odot$	(D model*);	242±61 $R_\odot$	(P model**)
Theoretical linear Rosseland radii $R_{\rm m}$:	246 $R_\odot$	(D model*);	263 $R_\odot$	(P model**)
Measured linear R Aql stellar K-band radii $R_{\rm K,m}$:	253±64 $R_\odot$	(D model*);	238±61 $R_\odot$	(P model**)
Theoretical linear stellar K-band radii $R_{\rm K,m}$:	241 $R_\odot$	(D model*);	259 $R_\odot$	(P model**)
Measured R Aql effective temperature:	3007±155 K	(D model*);	3109±168 K	(P model**)
Theoretical effective temperature:	3025 K	(D model*);	3030 K	(P model**)

(* average over phases 1.0, 2.0; ** average over phases 1.0, 2.0, 3.0, 4.0)

The comparison suggests that R Aql is well represented by the fundamental mode D and P model (BSW96, HSW98). The measured Rosseland radius of $R = 250 \pm 63\,R_\odot$ (average of the derived values from D and P model CLVs; corresponding theoretical D/P model Rosseland radius $= 255\,R_\odot$) places R Aql among the fundamental mode pulsators in the period-radius relation which also is in agreement with Ref. 8. Note, however, that observations in more filters than just one continuum filter may be necessary for safely distinguishing a well-fitting model from an accidental match (cf. Ref. 10).

5. REFERENCES

1. M.S. Bessell, M. Scholz, P.R. Wood, *A&A* **307**, pp. 481, 1996 (BSW96)
2. K.-H. Hofmann, M. Scholz, P.R. Wood, *A&A* **339**, pp. 846, 1998 (HSW98)
3. D. Bonneau, A. Labeyrie, *ApJ* **181**, pp. L1, 1973
4. M. Karovska, P. Nisenson, C. Papaliolios, R.P. Boyle, *ApJ* **374**, pp. L51, 1991
5. A. Quirrenbach, D. Mozurkewich, J.T. Armstrong, et al., *A&A* **259**, pp. L19, 1992
6. C.A. Haniff, M. Scholz, P.G. Tuthill, *MNRAS* **276**, pp. 640, 1995
7. G. Weigelt, Y. Balega, K.-H. Hofmann, M. Scholz, *A&A* **316**, pp. L21, 1996
8. G.T. Van Belle, H.M. Dyck, J.A. Benson, M.G. Lacasse, *AJ* **112**, pp. 2147, 1996
9. G. Perrin, V. Coudé du Foresto, S.T. Ridgway, et al., *A&A* **345**, pp. 221, 1999
10. K.-H. Hofmann, Y. Balega, M. Scholz, G. Weigelt, *A&A* **353**, pp. 1016, 2000
11. T. Watanabe, K. Kodaira, *PASJ* **31**, pp. 61, 1979
12. M. Scholz, *A&A* **145**, pp. 251, 1985
13. M.S. Bessell, J.M. Brett, M. Scholz, P.R. Wood, *A&A* **213**, pp. 209, 1989
14. N.P. Carleton, W.A. Traub, M.G. Lacasse, et al., *Proc. SPIE* **2200**, pp. 152, 1994
15. W.A. Traub, et al., *Proc. SPIE* **3350**, pp. 848, 1998
16. V. Coudé du Foresto, S.T. Ridgway, J.-M. Mariotti, *A&AS* **121**, pp. 379, 1997
17. G. Perrin, V. Coudé du Foresto, S.T. Ridgway, et al. *A&A* **331**, pp. 619, 1998
18. H.M. Dyck, J.A. Benson, G.T. Van Belle, S.T. Ridgway, *AJ* **111(4)**, pp. 1705, 1996
19. M. Scholz, Y. Takeda, *A&A* **186**, pp. 200, 1987 (erratum: 196, 342)
20. F. Van Leeuwen, M.W. Feast, P.A. Whitelock, B. Yudin, *MNRAS* **287**, pp. 955, 1997
21. M.W. Fox, P.R. Wood, *ApJ* **259**, pp. 198, 1982